

Supporting information for

Semimetallic Molybdenum Disulfide Ultrathin Nanosheets as An Efficient Electrocatalyst for Hydrogen Evolution

Xu Sun[†], Jun Dai[§], Yuqiao Guo[†], Changzheng Wu^{*†}, Fanting Hu[†], Jiyin Zhao[†],
Xiaocheng Zeng[§], Yi Xie^{*†}

Table of contents

S1. The volcano curve reported for most common catalyst materials	2
S2. Structural information and density functional calculations for the MoS₂ bulk and V-doped MoS₂ monolayer structures	3
S3. Characterization of the as-synthesized V-doped MoS₂ bulk samples	4
S4. Characterization of the VMS nanosheet.....	7
S5. Characterization of the assembled VMS thin film.....	9
S6. M-H curves of VMS nanosheet.....	10
S7. Characterization of the pure MoS₂ nanosheet	11
S8. XRD patterns of VMS with a higher V/Mo ratio.....	12
S9. XPS analysis of VMS catalyst before and after HER process.	13
S10. Catalytic properties of VMS and pure MoS₂ catalyst	14

S1. The volcano curve reported for most common catalyst materials

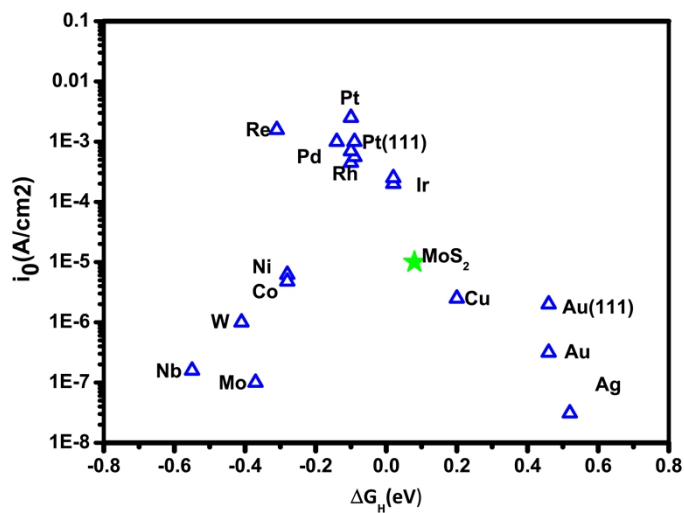


Figure S1. The volcano curve for the most common catalyst materials. As presented in the volcano plot, the exchange current density is as a function of the free energy of adsorption of hydrogen calculated by DFT.^[1,2] The appropriate hydrogen binding energy of MoS₂, which is located close to the top of the volcano curve, illustrates the probability of MoS₂ acting as an advanced catalyst in the electrochemical reaction.

S2. Structural information and density functional calculations for the MoS₂ bulk and V-doped MoS₂ monolayer structures

Molybdenum disulfide (MoS₂) is a hexagonal crystal with layered structure stacked by S-Mo-S alternating layers. 2H-MoS₂ based on D3h-MoS₆ units, for which unit cell include two S-Mo-S monolayers, is dominant and more stable with cell parameters *a* and *c* of 3.15 Å and 12.3 Å, respectively. In this structure, the Mo atoms occupied the triangular prism sites in between the hexagonal closed-packed layer of S atoms. The adjacent layers were connected by the weak van der Waals interactions, bringing the exfoliative characteristic of this compound.

The electronic band structure was studied with density functional theory (DFT) calculations. The periodic boundary condition plane wave basis-set code package VASP was adopted. The electron-ion interaction was described by the projector augmented-wave (PAW) method. The exchange-correlation energy was described by the Perdew-Burke-Ernzerhof (PBE) functional. The energy cutoff was set to 500 eV. For geometric optimization, both lattice constants and atomic positions are relaxed until the forces on atoms are less than 0.02 eV/Å and the total energy change is less than 1.0×10⁻⁵ eV. K (1/3, 1/3, 0.0), G (0.0, 0.0, 0.0) and M (0.5, 0.0, 0.0) refer to the special points in the first Brouillon zone.

As is shown in **Figure S2**, the calculation results revealed that the pristine 2H-MoS₂ nanosheet is mott insulator; while for the monolayer of VMS, the PBE calculations give a semimetal character.

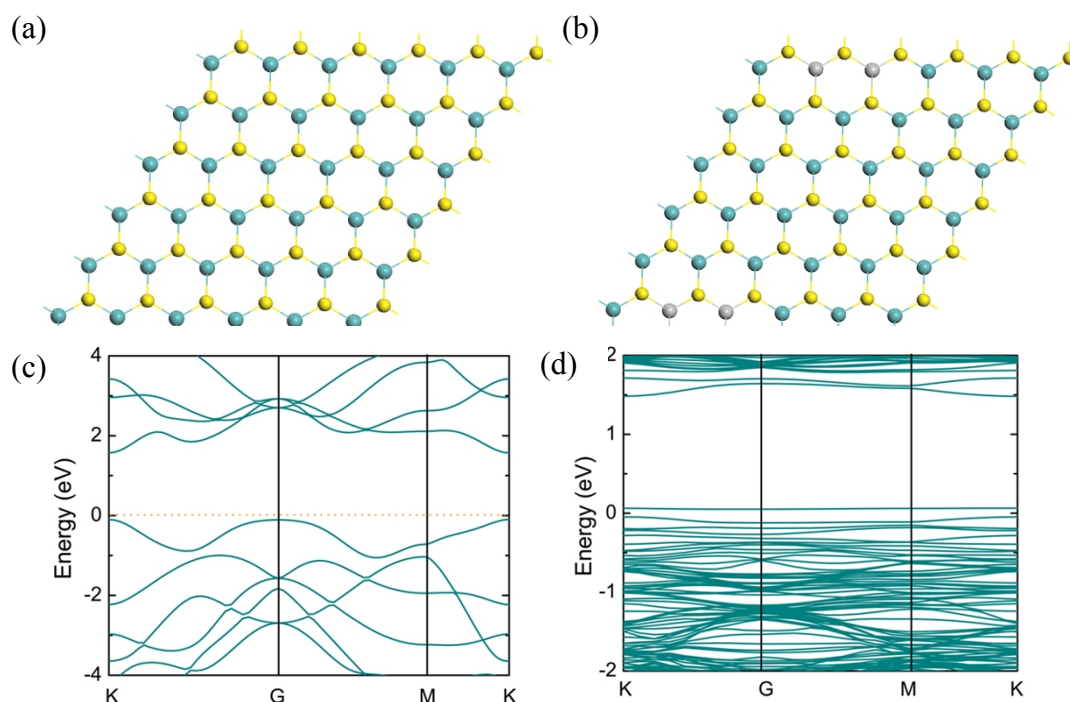


Figure S2. (a) and (b) Atomic structure of 2H-MoS₂ and V_{0.08}Mo_{0.92}S₂ nanosheets along c-axis respectively, showing the notable two-dimensional structure; The band structure of (c) MoS₂ nanosheet calculated with PBE functional based on the structure of (a), and (d) V_{0.08}Mo_{0.92}S₂ monolayer calculated with PBE functional based on the monolayer structure of (b).

S3. Characterization of the as-synthesized V-doped MoS₂ bulk samples

S3.1 X-ray diffraction analysis

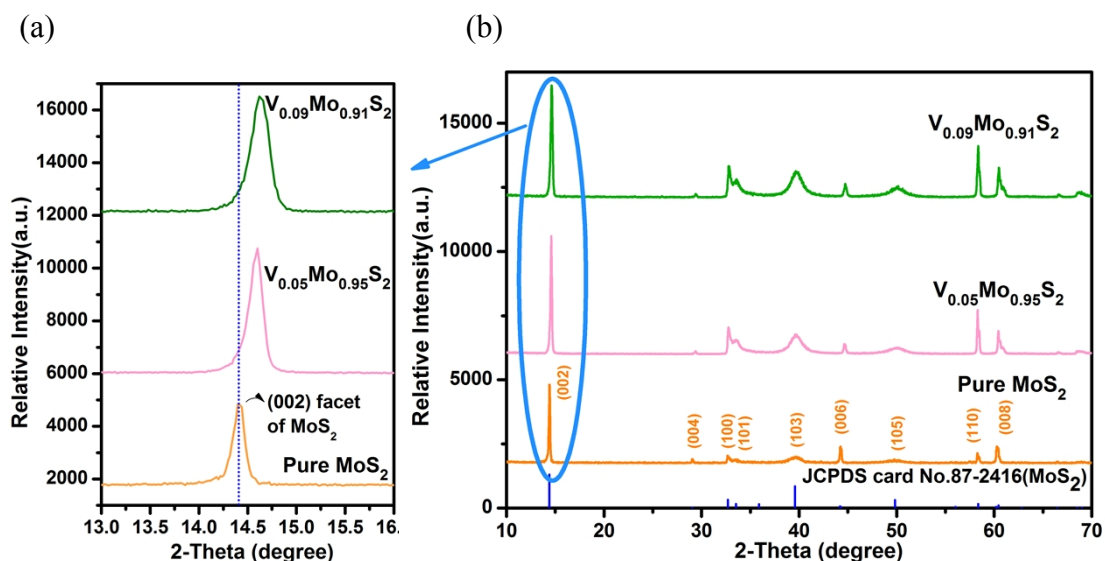


Figure S3. XRD pattern of bulk V_{0.09}Mo_{0.91}S₂, V_{0.05}Mo_{0.95}S₂ and pure MoS₂, respectively. (a) Magnification of the circled area in (b), which shows substantial shifts of the (002) facet along c axis, indicating the gradual reduced (002) facet spacing. This reduction is mainly due to the smaller ionic radii of V⁴⁺ (72pm) compared with Mo⁴⁺ (79pm). Of note, the samples were fully grounded to avoid orientation for better phase identification. No other characteristic reflection peaks were observed, demonstrating that the V atom was successfully incorporated into the lattice structure of MoS₂ and no noticeable impurities existed in the product.

S3.2 Morphological characterization of bulk $V_{0.05}Mo_{0.95}S_2$ and $V_{0.09}Mo_{0.91}S_2$ samples

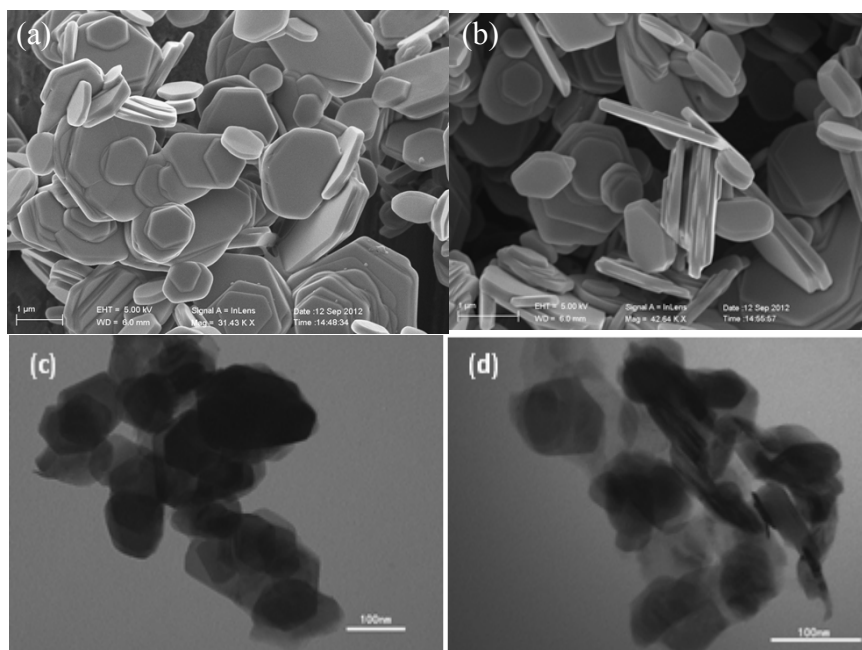


Figure S4. Characterization of the as-synthesized bulk VMS samples. (a) and (b) SEM images of $V_{0.05}Mo_{0.95}S_2$ and $V_{0.09}Mo_{0.91}S_2$, respectively. As is presented in the images, all the synthesized samples are uniform thick plates with the thickness of about 100nm. And along with the increment of vanadium concentration, the thick plates became smaller, that might be caused by in-plane doping. (c) and (d) TEM images of $V_{0.05}Mo_{0.95}S_2$ and $V_{0.09}Mo_{0.91}S_2$ dispersed in ethanol for characterization, from which the black part demonstrates the large thickness of the VMS bulk.

S3.3 HRTEM and EDS mapping of the bulk $V_{0.09}Mo_{0.91}S_2$

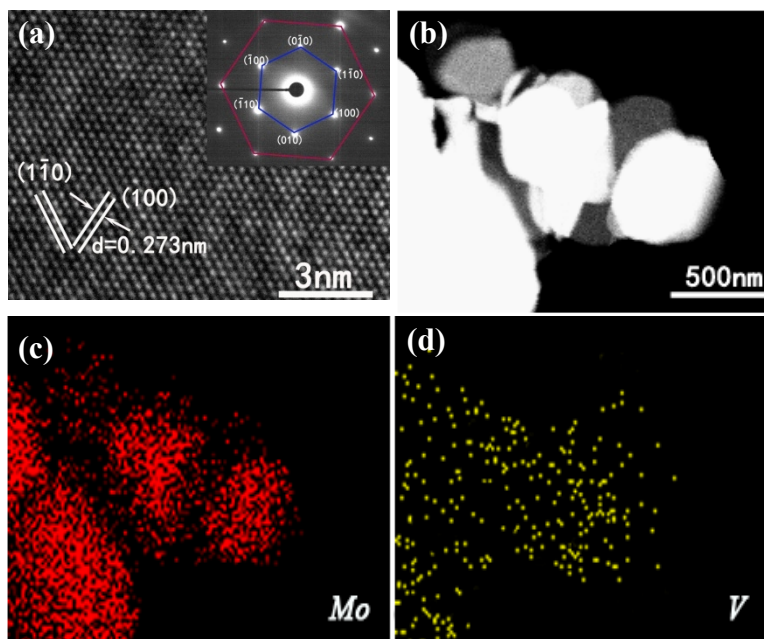


Figure S5. (a) HRTEM and SA-ED patterns of the synthesized $V_{0.09}Mo_{0.91}S_2$ bulk samples. The interplanar distance of 2.73 Å matched well with the plane distances of d_{100} and d_{010} , respectively, of the facets of MoS_2 . The well kept interplanar distance illustrated the incorporation of vanadium atoms in the basal plane, excluding the intercalation between two adjacent layers. The hexagonal symmetry as well as the orientation values of 60° of the two planes of (010) and (100) in the SAED patterns demonstrated the well kept hexagonal crystal structure. The typical HAADF-STEM (b) and elemental mapping images (c, d) of bulk $V_{0.09}Mo_{0.91}S_2$, where the elements of Mo (indicated by red color) and V (indicated by yellow color) were homogenously spatial distributions, illustrated the successful incorporation of vanadium atoms into the MoS_2 lattice.

S4. Characterization of the VMS nanosheet

S4.1 Morphological characterizations of the exfoliated nanosheet

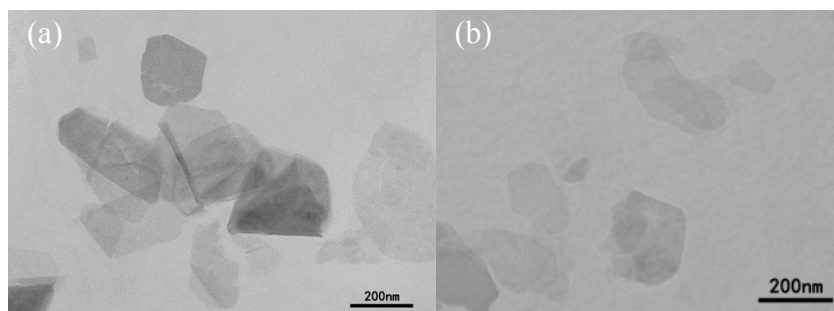


Figure S6. Characterizations of exfoliated VMS ultrathin nanosheets. (a) and (b) TEM image of $V_{0.05}Mo_{0.95}S_2$ and $V_{0.09}Mo_{0.91}S_2$, respectively, from which, the well dispersion and the ultrathin characteristics can be clearly seen, demonstrating the successful exfoliation of bulk samples into the ultrathin nanosheets.

S4.2 Elemental analysis of the VMS nanosheet by HRTEM

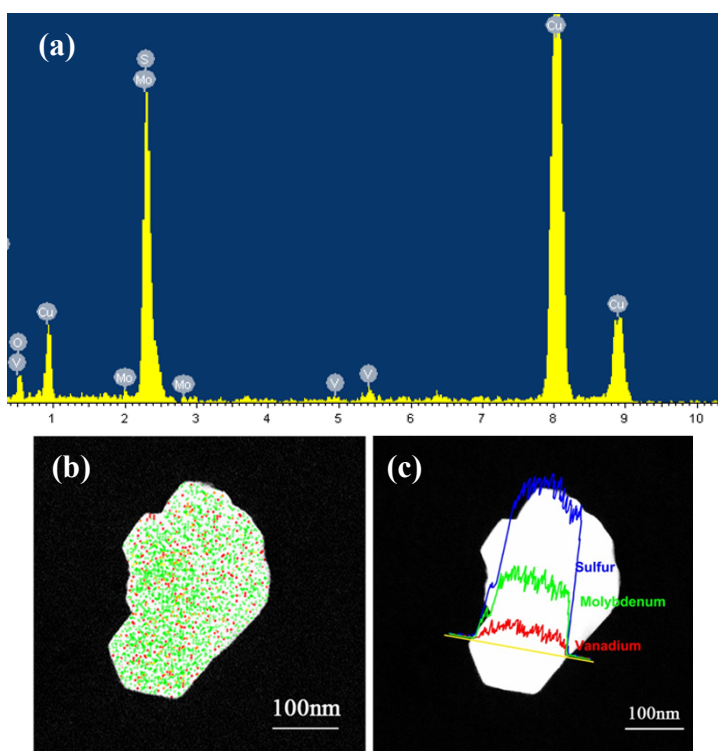


Figure S7. (a) Energy-dispersive spectroscopy (EDS) of a typical ultrathin nanosheet, where the signals of Cu are generated from the Cu grids. (b) Overlapped elemental mapping of Mo and V in $V_{0.09}Mo_{0.91}S_2$ nanosheet. (c) EDS line scanning profiles of $V_{0.09}Mo_{0.91}S_2$ ultrathin nanosheet. The EDS mapping and spectrum confirm the product has the chemical formula of $V_xMo_{1-x}S_2$, with no other obvious contaminants existed in the as-obtained nanosheets.

S4.3 Thickness and lateral size distribution of the VMS nanosheets

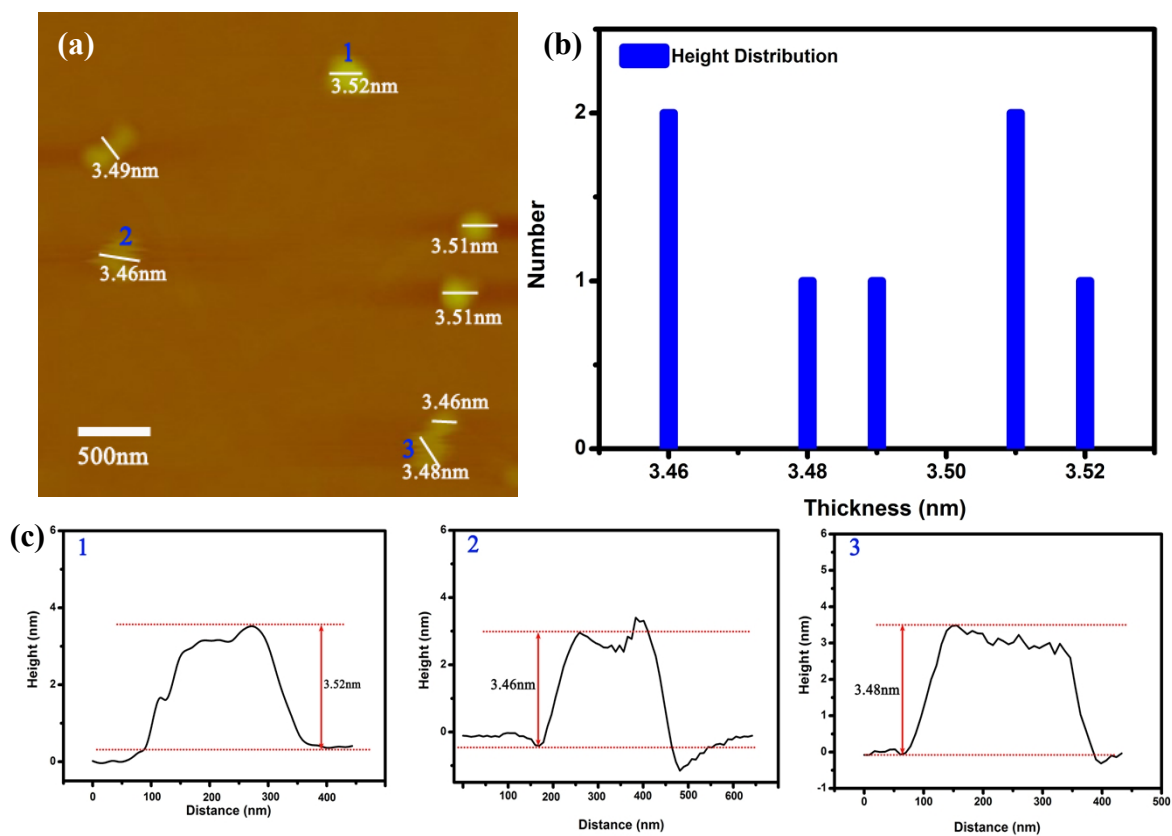


Figure S8. (a) AFM image of the VMS nanosheets and height parameters of each nanosheet; (b) Thickness distribution of the VMS nanosheets; (c) Height profiles, the numbers 1, 2 and 3 in c correspond to the numbers 1, 2 and 3 in a.

S5. Characterization of the assembled VMS thin film

S5.1 Surface morphology and cross section of the assembled VMS film

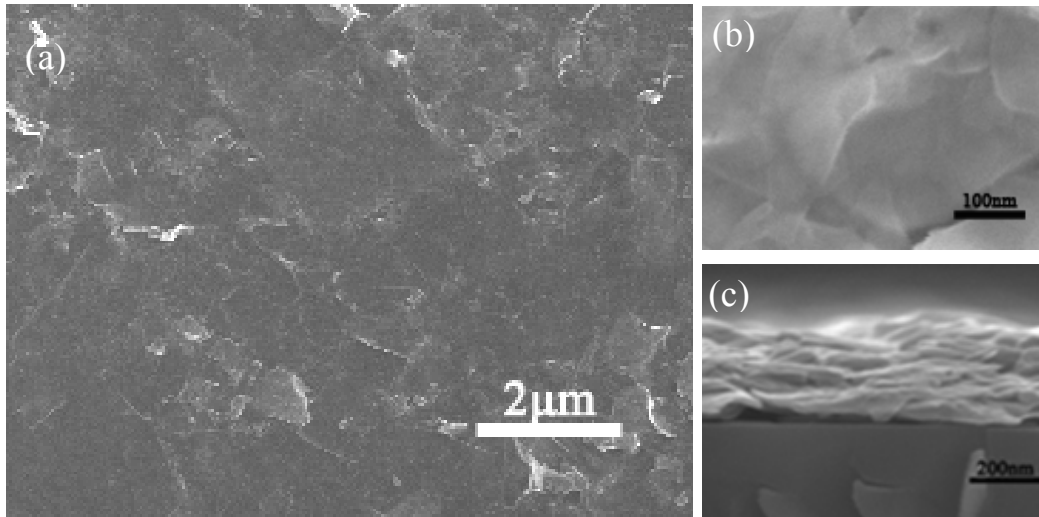


Figure S9. SEM images of assembled VMS ultrathin nanosheet films. (a) Low-magnification SEM image of surface morphology for the assembled VMS thin film, from which a smooth surface can be clearly seen, thus demonstrating the tightly compressed character. (b) High-magnification SEM image of the thin film assembled from the VMS nanosheets. (c) Cross-section of the as-assembled film based on the exfoliated ultrathin nanosheets, showing their layer-by-layer overlapping outlook.

S5.2 Raman spectra of the VMS assembled films

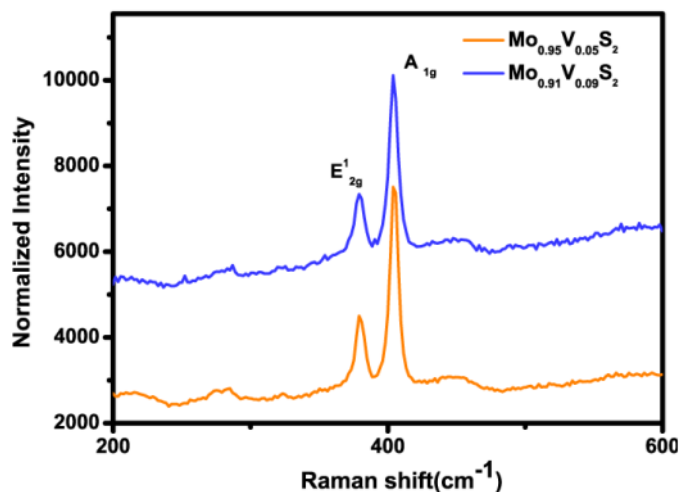


Figure S10. The Raman spectra of the two assembled VMS films with chemical formula of $V_{0.05}Mo_{0.95}S_2$ and $V_{0.09}Mo_{0.91}S_2$, respectively. As shown in the Figure S10, two-prominent peaks corresponding to the in-plane E_{2g}^1 and out-plane A_{1g} modes of 2H-MoS₂ can be clearly seen in these two samples. Both peaks' positions matched well with the reported 2H-MoS₂ with no noticeable differences between them.³⁻⁵ And the broadening of Raman peaks can be attributed to the inhomogeneity of the VMS thin films.

S5.3 Mo3d XPS spectra of VMS nanosheet

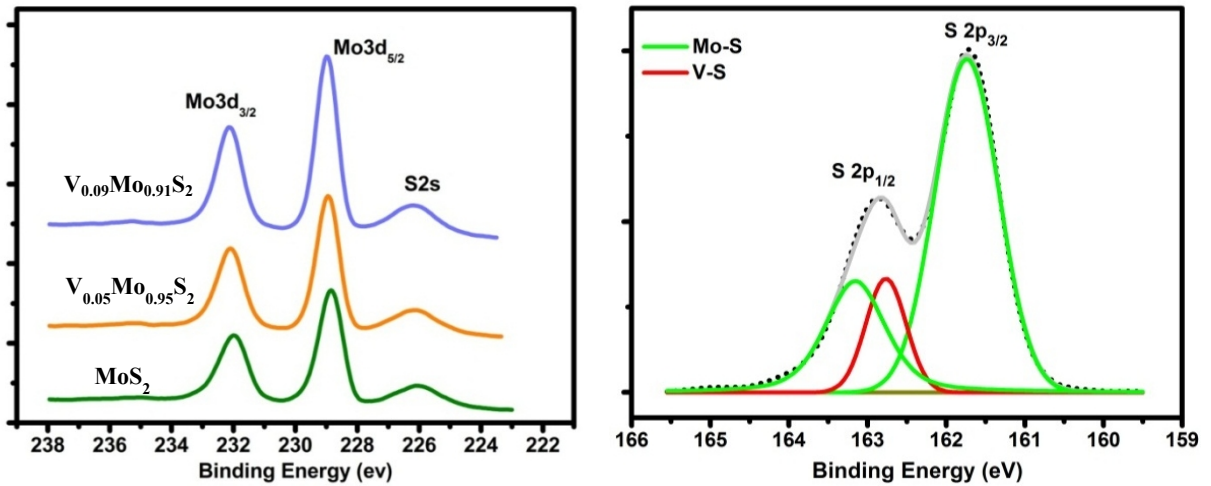


Figure S11. (a) Representative Mo 3d XPS spectra of pure MoS_2 and VMS samples with different Mo/V ratios. (b) S 2p XPS spectra of $V_{0.09}Mo_{0.91}S_2$ sample.

S6. M-H curves of VMS nanosheets

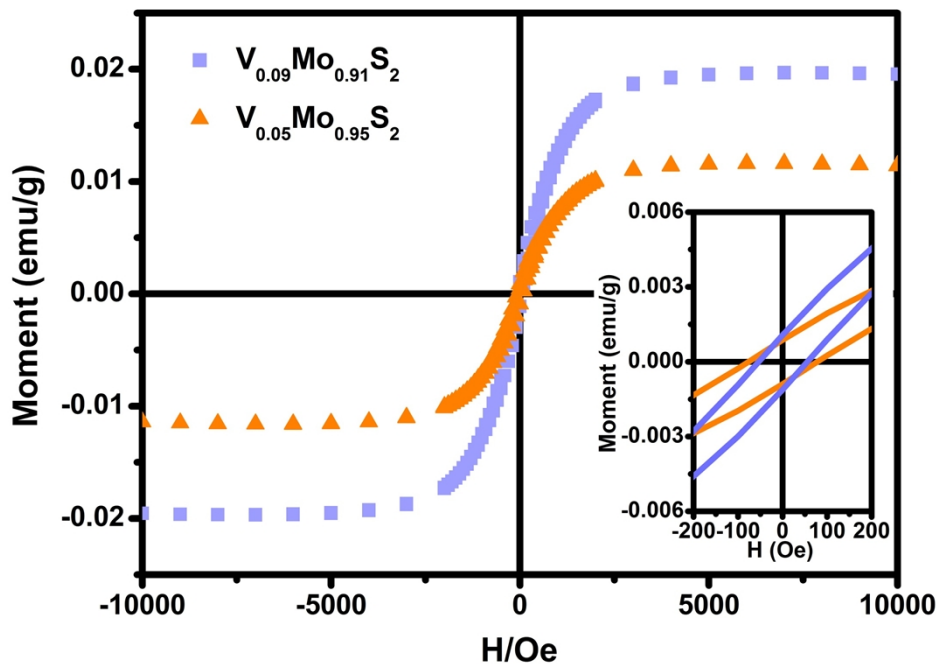


Figure S12. Magnetic-field dependence of magnetization curve of the synthetic VMS nanosheets at 300K. Since the pure MoS_2 is paramagnetic, the observed room-temperature ferromagnetism here should be induced by the intralayer-doped vanadium atoms, demonstrating the successful incorporation of vanadium atoms. Inset: enlarged central section of M-H curve

S7. Characterization of the pure MoS₂ nanosheet

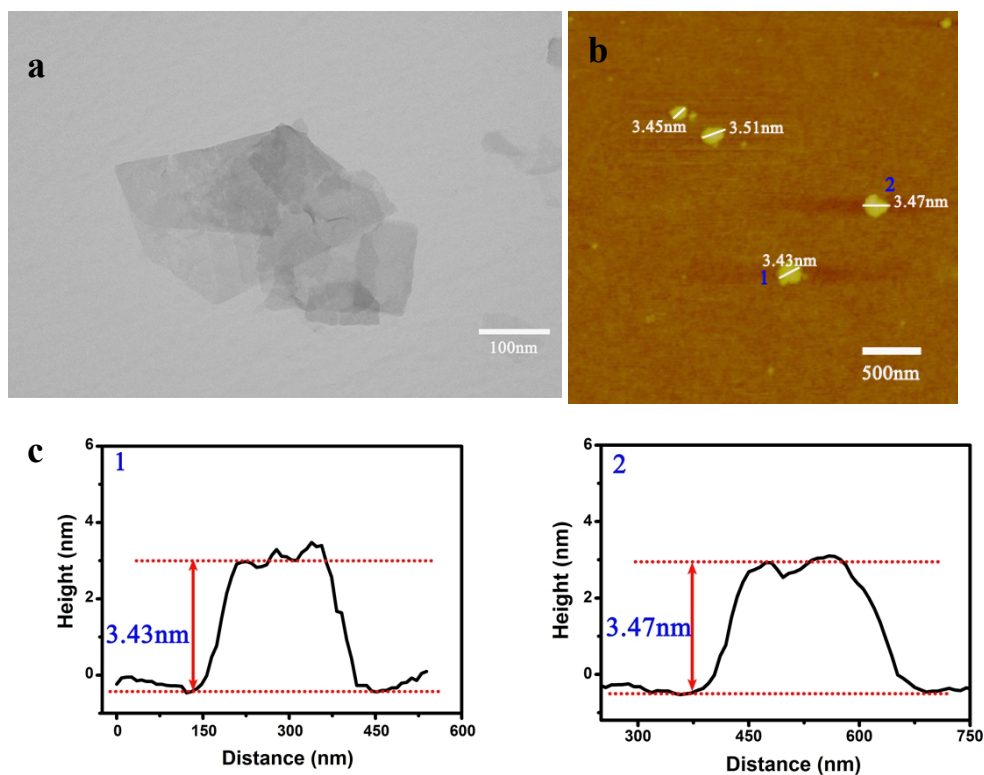


Figure S13. Characterizations of exfoliated pure MoS₂ ultrathin nanosheets. (a) TEM image of MoS₂ nanosheet, from which, the well dispersion and the ultrathin characteristics can be clearly seen, demonstrating the successful exfoliation of bulk samples into the ultrathin nanosheets. (b) AFM image of the MoS₂ nanosheets and the height parameters of the individual nanosheets. (c) Height profiles, the numbers 1 and 2 in c correspond to the numbers 1 and 2 in b, respectively.

S8. XRD patterns of VMS with a higher V/Mo ratio.

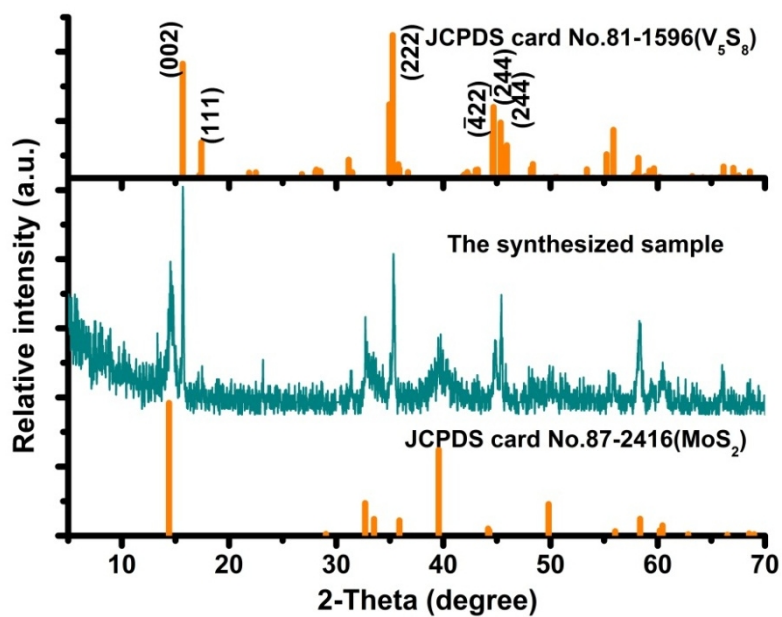


Figure S14. XRD pattern of synthesized sample with a higher V/Mo ratio of 1/3. The peak located at 15.68° was subjected to the (002) facet of V_5S_8 .

S9. XPS analysis of VMS catalyst before and after HER process.

Table S1 Binding energies of V2p_{3/2} and V2p_{1/2}

Formula Spectral line	VO ₂	V ₂ O ₅	BaVS ₃
V2p _{1/2}	524.2eV	524.8eV	
V2p _{3/2}	516.5eV	517eV	514.3eV

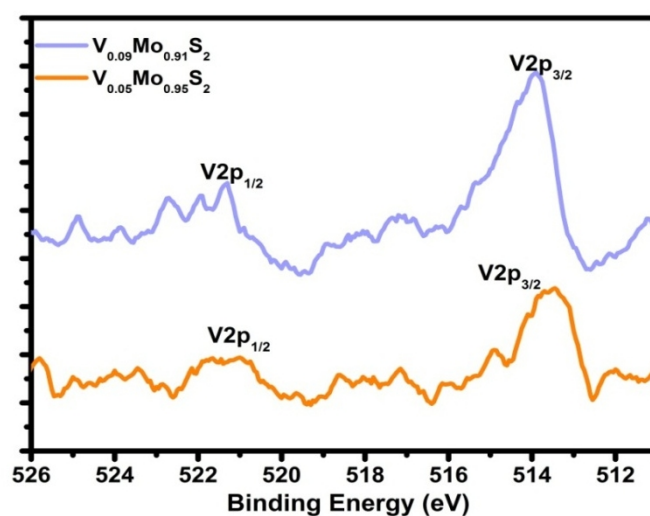


Figure S15. Representative V2p XPS spectra of VMS catalysts after HER process.

Table S2 The At.% values obtained from the XPS analysis of VMS catalysts before and after HER process

	Before the HER experiment				After the HER experiment			
	At%		V/Mo ratio	V _x MoS ₂	At%		V/Mo ratio	V _x MoS ₂
	V	Mo			V	Mo		
Sample1	1.84	21.19	0.087	V _{0.08} Mo _{0.92} S ₂	1.8	21.44	0.083	V _{0.08} Mo _{0.92} S ₂
Sample2	1.21	24.28	0.050	V _{0.05} Mo _{0.95} S ₂	1.22	21.69	0.056	V _{0.05} Mo _{0.95} S ₂

S10. Catalytic properties of VMS and pure MoS₂ catalyst

S10.1 Polarization current analysis of VMS and pure MoS₂ catalyst

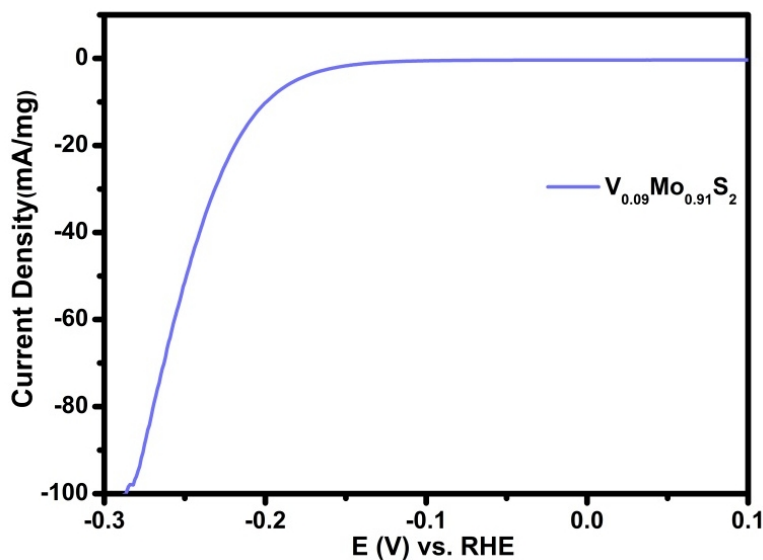


Figure S16. Polarization curve of the V_{0.09}Mo_{0.91}S₂ nanosheet catalyst with the current density normalized by the loading weight.

Table S3. HER parameters of VMS nanosheet catalyst and pure MoS₂ samples

Catalyst	Tafel slope [mV/decade]	j [mA cm ⁻²] [a]
V _{0.09} Mo _{0.91} S ₂	69	32.47
V _{0.05} Mo _{0.95} S ₂	80	17.81
MoS ₂ nanosheet	90	2.66
Bulk MoS ₂	120	0.31

a. Current densities at $\eta = 0.29$ V

The experimental conditions for the above catalysts, such as catalyst loading, scan rate as well as the solution environment, are all the same.

S10.2 Detail Analysis of the equivalent circuit

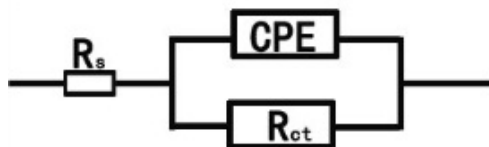


Figure S17. The catalytic system is described by this simple equivalent electrical circuit. R_s represents the uncomposed solution resistance of the system. It can be read from the intercept of the semicircle on the real axis in the Nyquist plot. R_{ct} is attributed to charge transfer resistance. A constant phase element (CPE) was also employed representing the double-layer capacitance under HER conditions.^{6,7}

S10.3 IR-corrected Catalyst Activity

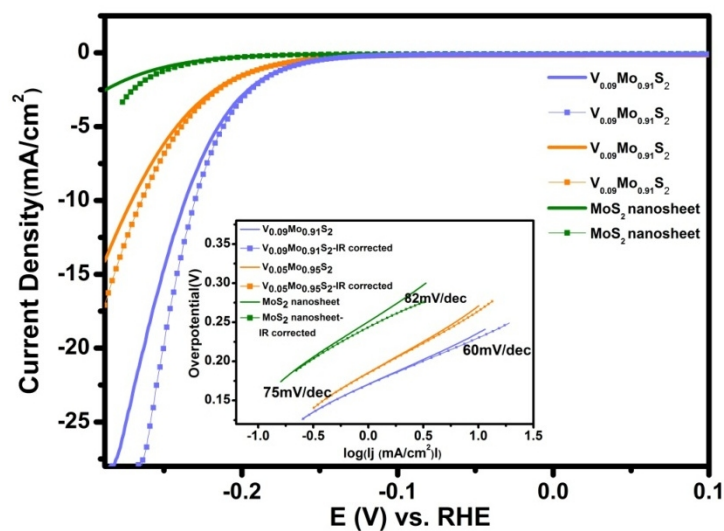


Figure S18. Polarization curves showing the raw and iR-corrected catalytic activity of VMS nanosheet and MoS₂ nanosheet catalyst. The iR correction is performed by $\eta_{\text{corr}} = \eta - jR_s$ (j represents the polarization current) based on the corresponding R_s . Inset: The corresponding Tafel plots.⁸

S10.4 Nyquist plot of $V_{0.09}Mo_{0.91}S_2$ nanosheet catalyst under various overpotentials

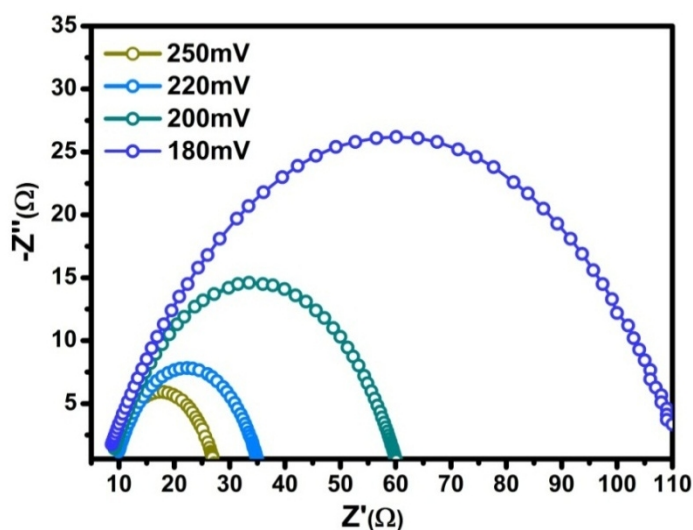


Figure S19. Nyquist plots of VMS nanosheet catalyst at various overpotentials of 180mV, 200mV, 220mV and 250mV. The solution resistance was overpotential independent about 8~9Ω, while the R_{ct} decreased with the increment of the overpotential.

S10.5 The continuous HER process at static overpotential

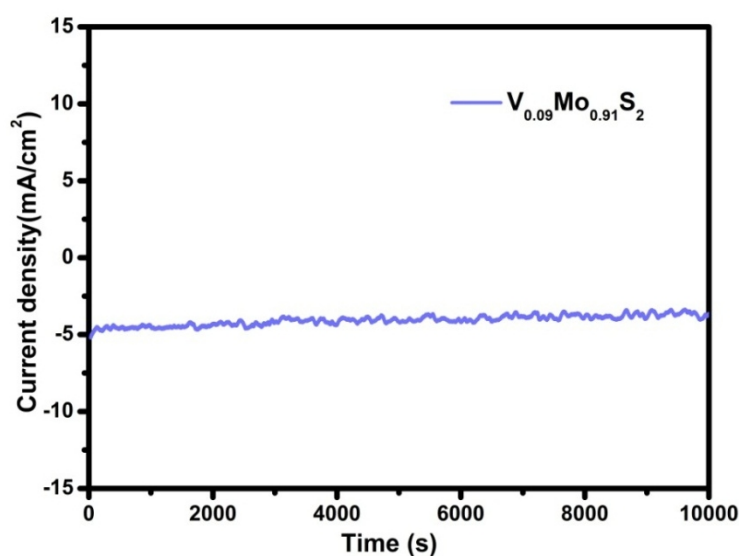


Figure S20. Time dependence of current density under static overpotential of 200 mV. Under the overpotential of 200 mV, continuous HER process occurred. The as-obtained time-dependent curve is in serrate shape, which should be attributed to the accumulation and release of the hydrogen bubble. The slightly degradation of the current density after a long period of 10000 seconds might be caused by the consumption of H^+ or the remaining of H_2 bubbles on the electrode.

S10.6 The catalytic activities of VMS nanosheet catalysts and the bulk VMS catalyst

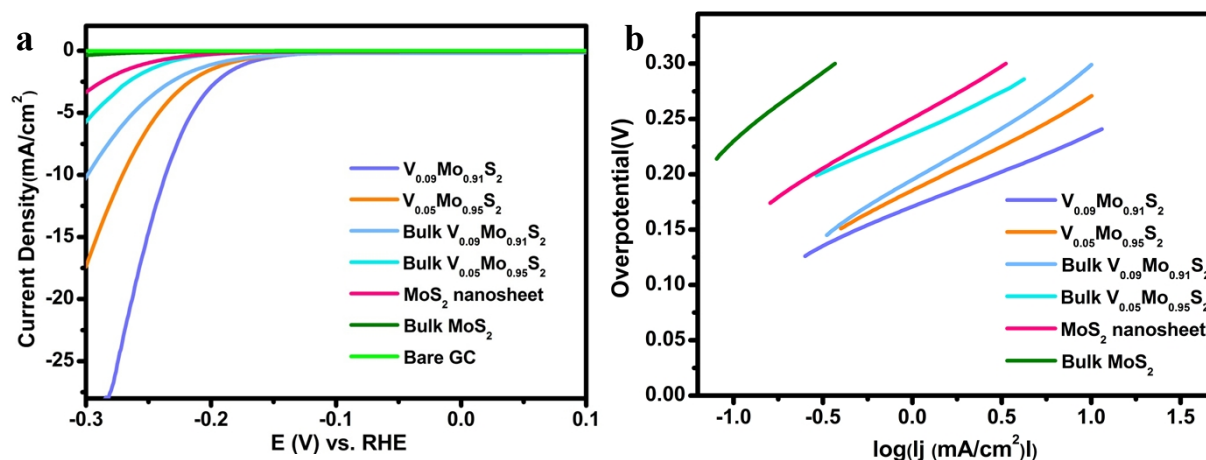


Figure S21. (a) Polarization curves recorded on decorated GC electrode consisting of various VMS nanosheet catalysts and the bulk VMS catalyst. (b) The corresponding Tafel plots derived from (a).

S10.7 The relevant cyclic voltammograms of VMS and pure MoS₂ nanosheet.

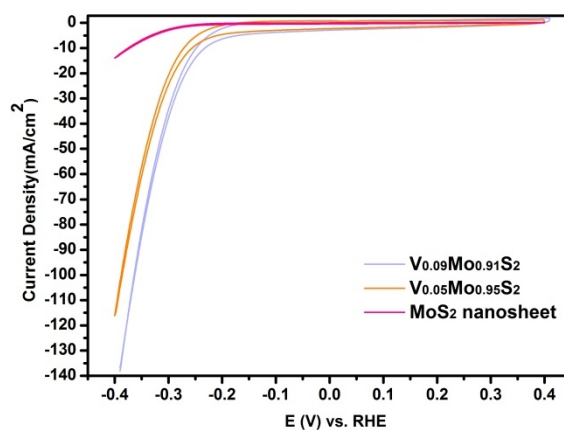


Figure S22: The relevant cyclic voltammograms of different VMS nanosheets and pure MoS₂ nanosheets. It can be seen clearly that no redox peaks appeared in the VMS catalysts, which are the same with the pure MoS₂ catalyst, illustrating that the the incorporation of vanadium atoms didn't cause any redox reactions in the HER process.

References:

1. Trasatti, S., Work function, electronegativity, and electrochemical behaviour of metals: II. Potentials of zero charge and “electrochemical” work functions. *J. Electroanal. Chem. Interfac.* **1971**, *33*, 351-378.
2. Jaramillo, T. F.; Jørgensen, K. P.; Bonde, J.; Nielsen, J. H.; Horch, S.; Chorkendorff, I., Identification of Active Edge Sites for Electrochemical H₂ Evolution from MoS₂ Nanocatalysts. *Science* **2007**, *317*, 100-102.
3. Ramakrishna Matte, H. S. S.; Gomathi, A.; Manna, A. K.; Late, D. J.; Datta, R.; Pati, S. K.; Rao, C. N. R., MoS₂ and WS₂ Analogues of Graphene. *Angew. Chem. Int. Ed.* **2010**, *49*, 4059-4062.
4. Zeng, Z.; Yin, Z.; Huang, X.; Li, H.; He, Q.; Lu, G.; Boey, F.; Zhang, H., Single-Layer Semiconducting Nanosheets: High-Yield Preparation and Device Fabrication. *Angew. Chem. Int. Ed.* **2011**, *50*, 11093-11097.
5. Li, H.; Zhang, Q.; Yap, C. C. R.; Tay, B. K.; Edwin, T. H. T.; Olivier, A.; Baillargeat, D., From Bulk to Monolayer MoS₂: Evolution of Raman Scattering. *Adv. Funct. Mater.* **2012**, *22*, 1385-1390.
6. Merki, D.; Vrubel, H.; Rovelli, L.; Fierro, S.; Hu, X., Fe, Co, and Ni ions promote the catalytic activity of amorphous molybdenum sulfide films for hydrogen evolution. *Chem. Sci.* **2012**, *3*, 2515-2525.
7. Liao, L.; Zhu, J.; Bian, X.; Zhu, L.; Scanlon, M. D.; Girault, H. H.; Liu, B., MoS₂ Formed on Mesoporous Graphene as a Highly Active Catalyst for Hydrogen Evolution. *Adv. Funct. Mater.* **2013**, DOI: 10.1002/adfm.201300318.
8. Chen, Z.; Cummins, D.; Reinecke, B. N.; Clark, E.; Sunkara, M. K.; Jaramillo, T. F., Core-shell MoO₃-MoS₂ Nanowires for Hydrogen Evolution: A Functional Design for Electrocatalytic Materials. *Nano Letters.* **2011**, *11*, 4168-4175.